Superconductivity and Lattice Instability in Compressed Lithium from Fermi Surface Hot Spots

Deepa Kasinathan,[1] J. Kuneš,[1,2] A. Lazicki,[1,3] H. Rosner,[4] C. S. Yoo,[3] R. T. Scalettar,[1] and W. E. Pickett[1]

[1]*Department of Physics, University of California–Davis, Davis, California 95616, USA*
[2]*Institute of Physics, ASCR, Cukrovarnická 10, 162 53 Praha 6, Czech Republic*
[3]*Lawrence Livermore National Laboratory, Livermore, California 94551, USA*
[4]*Max-Planck-Institüt für Chemische Physik fester Stoffe, Dresden, Germany*

(Received 5 August 2005; published 2 February 2006)

The highest superconducting temperature T_c observed in any elemental metal (Li with $T_c \sim 18$–20 K at pressure 35–48 GPa) is shown to arise from increasingly strong electron-phonon coupling concentrated along intersections of Kohn anomaly surfaces with the evolving Fermi surface. First-principles linear response calculations of the phonon spectrum and spectral function $\alpha^2F(\omega)$ reveal very strong Q- and phonon-polarization dependence of coupling strength, resulting in values of T_c in the observed range. The sharp momentum dependence of the coupling even for the simple Li Fermi surface indicates more generally that a fine Q mesh is required for precise evaluation of λ.

DOI: 10.1103/PhysRevLett.96.047004 PACS numbers: 74.70.Ad, 74.25.Jb, 74.25.Kc, 74.62.Fj

The recent observations of superconductivity in fcc Li up to $T_c = 14$ K in near-hydrostatic fcc-phase samples [1], and as high as 20 K in nonhydrostatic pressure cells [2,3], in the pressure (P) range 20–50 GPa provides almost as startling a development as the discovery [4] in 2001 of $T_c = 40$ K in MgB_2. Lithium at ambient conditions, after all, is a simple s-electron metal showing no superconductivity above 100 μK [5]. What can possibly lead to more than a 5 order of magnitude increase in T_c and transform it into the best elemental superconductor known, still in a simple, monatomic, cubic phase? There is little reason to suspect a magnetic (or other unconventional) pairing mechanism, but it seems equally unlikely that it transforms from a free-electron metal into a very strongly coupled electron-phonon (EP) superconductor at readily accessible pressures.

The strength of EP coupling in Li has attracted attention for some time. The empirical pseudopotential calculations of Allen and Cohen [6] suggested substantial coupling strength $\lambda = 0.56$ and, hence, readily observable superconductivity ($T_c > 1$ K). More recent calculations relying on the rigid muffin-tin approximation and phonon spectrum estimated from the Debye temperature reached a similar conclusion [7,8] and led Christensen and Novikov to predict a remarkably high $T_c \sim 70$ K under pressure [8]. Linear response calculations of the phonon spectrum and EP coupling by Liu *et al.* [9] in bcc Li confirmed that superconductivity would occur in bcc Li ($\lambda = 0.45$), but superconductivity is not observed due to the transformation into the 9R phase with 25% weaker coupling. Experimentally, superconductivity appears only above 20 GPa in the fcc phase [1–3].

In this Letter, we focus on the monatomic fcc phase that is stable in the 20–38 GPa range. After providing additional characterization of the previously discussed [10–13] evolution of the electronic structure under pressure, we analyze the implications of the Fermi surface (FS) topology for properties of Li. To study λ microscopically, Allen's decomposition [14] into mode coupling strengths $\lambda_{Q\nu}$ is used, where $\lambda = (1/3N)\sum_{Q\nu}\lambda_{Q\nu} = \langle\lambda_{Q\nu}\rangle$ is the Brillouin zone (BZ) and phonon branch (ν) average. Increase of pressure leads to very strong EP coupling to a specific branch in very restricted regions of momentum space determined by the FS topology; these features are directly analogous to the focusing of coupling strength [15–17] in MgB_2.

The volume at 35 GPa is 51% of that at $P = 0$, so the conduction electron density has doubled. We obtain a shift in character from s to p analogous to the $s \rightarrow d$ crossover in the heavier alkali metals [18]. The occupied bandwidth [19] increases by only 14% (much less than the free-electron value $2^{2/3} - 1 = 59\%$) because of compensation by a 55% increase in the $k = 0$ band mass ($m_b/m = 1.34$ at $P = 0$ to $m_b/m = 2.08$ at 35 GPa). At $P = 0$, the FSs are significantly nonspherical and just touch at the L points of the BZ. With increasing pressure, necks (as in Cu) appear along the $\langle 111\rangle$ directions, where the p character is strongest. The FS at 35 GPa is shown in Fig. 1, and its topology plays a crucial role in the superconductivity of Li.

The mode λ, given for $N_\nu = 3$ branches by

$$\lambda_{\vec{Q}\nu} = \frac{2N_\nu}{\omega_{\vec{Q}\nu}N(0)}\frac{1}{N}\sum_k |M^{[\nu]}_{k,k+Q}|^2\delta(\varepsilon_k)\delta(\varepsilon_{k+Q}), \quad (1)$$

is determined by the EP matrix elements $M^{[\nu]}_{k,k+Q}$ and the nesting function $\xi(Q)$ describing the phase space for electron-hole scattering across the FS ($E_F = 0$),

$$\xi(Q) = \frac{1}{N}\sum_k \delta(\varepsilon_k)\delta(\varepsilon_{k+Q}) \propto \oint \frac{d\mathcal{L}_k}{|\vec{v}_k \times \vec{v}_{k+Q}|}. \quad (2)$$

Here the integral is over the line of intersection of the FS and its image displaced by Q, $\vec{v}_k \equiv \nabla_k\varepsilon_k$ is the velocity, and $N(0)$ is the FS density of states. Evidently, $\xi(Q)$ gets

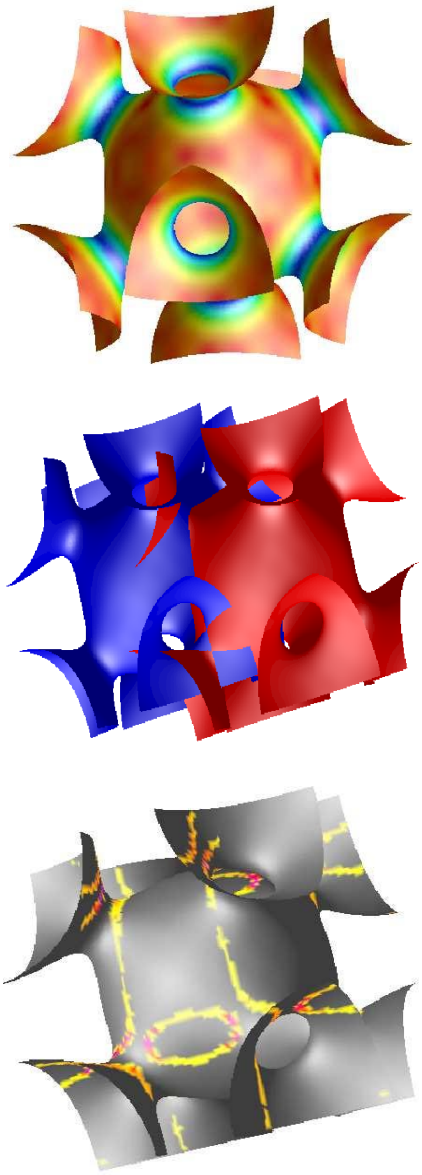

FIG. 1 (color online). Top: Fermi surface of Li at 35 GPa plotted in a cube region around $k = 0$ and colored by the value of the Fermi velocity. Red (belly areas) denotes fast electrons ($v_F^{\max} = 9 \times 10^7$ cm/s); blue (on necks) denotes the slower electrons ($v_F^{\min} = 4 \times 10^7$ cm/s) that are concentrated around the FS necks. The free-electron value is 1.7×10^8 cm/s. Middle: Fermi surfaces with relative shift of $0.71(1, 1, 0)$ (i.e., near the point K) indicating lines of intersection. Bottom: The light areas indicate the "hot spots" (the intersection of the Kohn anomaly surfaces with the Fermi surface) that are involved in strong nesting and strong coupling at $Q = 0.71(1, 1, 0)$ (see Fig. 2). These include the necks and three inequivalent lines connecting neck regions.

large if one of the velocities gets small or if the two velocities become collinear.

Note that $\frac{1}{N}\sum_Q \xi(Q) = [N(0)]^2$; the topology of the FS simply determines how the fixed number of scattering processes is distributed in Q. For a spherical FS, $\xi(Q) \propto \frac{1}{|Q|}\theta(2k_F - Q)$; in a lattice, it is a reciprocal lattice sum of such functions. This spherical FS behavior is altered dramatically in fcc Li, as shown in Fig. 2 for $P = 35$ GPa (the nonphysical and meaningless $\frac{1}{|Q|}$ divergence around Γ should be ignored). There is very fine structure in $\xi(Q)$ that demands a fine k mesh in the BZ integration, evidence that there is strong focusing of scattering processes around the K point, along the Γ-X line peaking at $\frac{3}{4}\,\Gamma$-$X \equiv X_K$, and also a pair of ridges (actually, cuts through surfaces) running in each (001) plane in K-X_K-K-X_K-K-X_K-K squares. Some additional structures are the simple discontinuities mentioned above, arising from the spherical regions of the FS.

Structure in $\xi(Q)$ arises where the integrand in Eq. (2) becomes singular, i.e., when the velocities at k and $k + Q$ become collinear. The FS locally is either parabolic or hyperbolic, and the nature of the singularity is governed by the difference surface (also either parabolic or hyperbolic). In the parabolic case (such as two spheres touching), $\xi(Q)$ has a discontinuity. In the hyperbolic case, however, $\xi(Q)$ diverges logarithmically. Such divergent points are not isolated but locally define a surface of such singularities (or discontinuities, in the parabolic case). The ridges and steps visible in Fig. 2 are cuts through

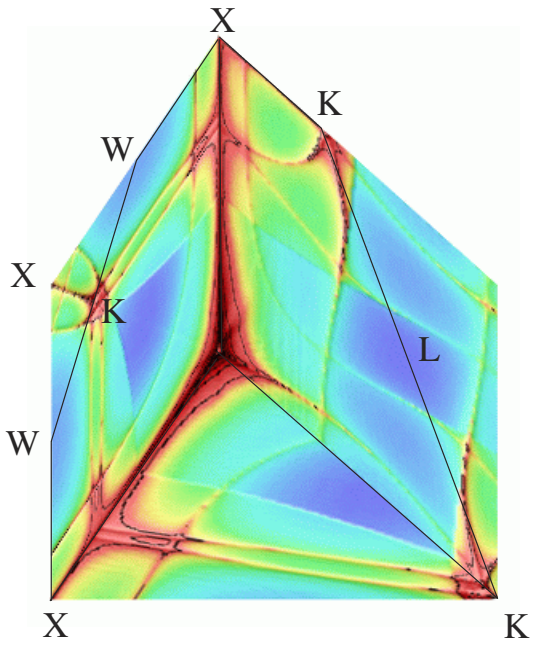

FIG. 2 (color online). Planar plots of the nesting function $\xi(Q)$ at 35 GPa throughout three symmetry planes: (010) Γ-X-W-K-W-X-Γ; (001) Γ-K-X-Γ; (110) Γ-K-L-K-X-Γ. The Γ point lies in the back corner. The dark (red) regions denote high intensity; the light (blue) regions denote low intensity. The maxima in these planes occur near K and along Γ-X. To obtain the fine structure, a cubic k mesh of $(2\pi/a)/160$ was used (2×10^6 points in the BZ).

these singular surfaces; the intensity at K arises from transitions from one neck to (near) another neck and is enhanced by the low neck velocity. Roth *et al.* have pointed out related effects on the susceptibility [20] (and, thus, the real part of the phonon self-energy), and Rice and Halperin [21] have discussed related processes for the tungsten FS. In the susceptibility (and the phonon renormalization), only FS nesting with antiparallel velocities gives rise to Q-dependent structure. This explains why the ridge in $\xi(Q)$ along the Γ-X line (due to transitions between necks and the region between necks) does not cause much softening (see below); there will, however, be large values of $\lambda_{Q\nu}$, because its structure depends only on collinearity.

Divergences of $\xi(Q)$, which are related to specific regions of the FS shown in the bottom panel in Fig. 1 (mostly distinct from the flattened regions between necks discussed elsewhere [13]), specify the Q regions of greatest instability. However, instabilities in harmonic approximation ($\omega_{Q\nu} \rightarrow 0$) may not correspond to physical instability. As the frequency softens, atomic displacements increase and the lattice can be stabilized to even stronger coupling (higher pressure) by anharmonic interactions, and, after all, the fcc structure is already close-packed. Thus, although we obtain a harmonic instability at $Q \sim K$ already at 25 GPa, it is entirely feasible that the system is anharmonically stabilized beyond this pressure, an example of anharmonically stabilized "high T_c" superconductivity.

The phonon energies and EP matrix elements have been obtained from linear response theory using Savrasov's full-potential linear muffin-tin orbital code [22]. Phonons are calculated at 72 inequivalent Q points (a $12 \times 12 \times 12$ grid), with a $40 \times 40 \times 40$ grid for the zone integration. To illustrate the evolution with pressure, we use the fcc lattice constants 8.00, 7.23, 6.80, and 6.41 bohr, corresponding approximately to 3, 10, 20, and 35 GPa, respectively, according to the experimental equation of state [23]. The 8.00 bohr value is the local-density approximation equilibrium lattice constant.

The phonon spectrum along Γ-X behaves fairly normally. The longitudinal ($\mathcal{L}$) branch at X hardens from 45 to 87 meV in the 0–35 GPa range, while the transverse ($\mathcal{T}$) mode at X remains at 30–35 meV. Along Γ-L, the behavior is somewhat more interesting: Again the $\mathcal{L}$ branch hardens as expected (40 → 84 meV), but the $\mathcal{T}$ branch remains low at 15–17 meV at the L point and acquires a noticeable dip near the midpoint, reflecting the ridge in $\xi(Q)$ running downward from the uppermost K point in Fig. 2. The important changes occur along the (110) Γ-K direction as shown in Fig. 3(a): The $\mathcal{L}$ and $\mathcal{T}_2$ branches harden conventionally, but the $\langle 1\bar{1}0\rangle$ polarized $\mathcal{T}_1$ branch softens dramatically around the point K, becoming unstable around 25 GPa. At 35 GPa, this mode is unstable in a substantial volume around the K point.

The EP spectral function $\alpha^2F(\omega)$ was evaluated using our mesh of 72 Q points and the tetrahedron method.

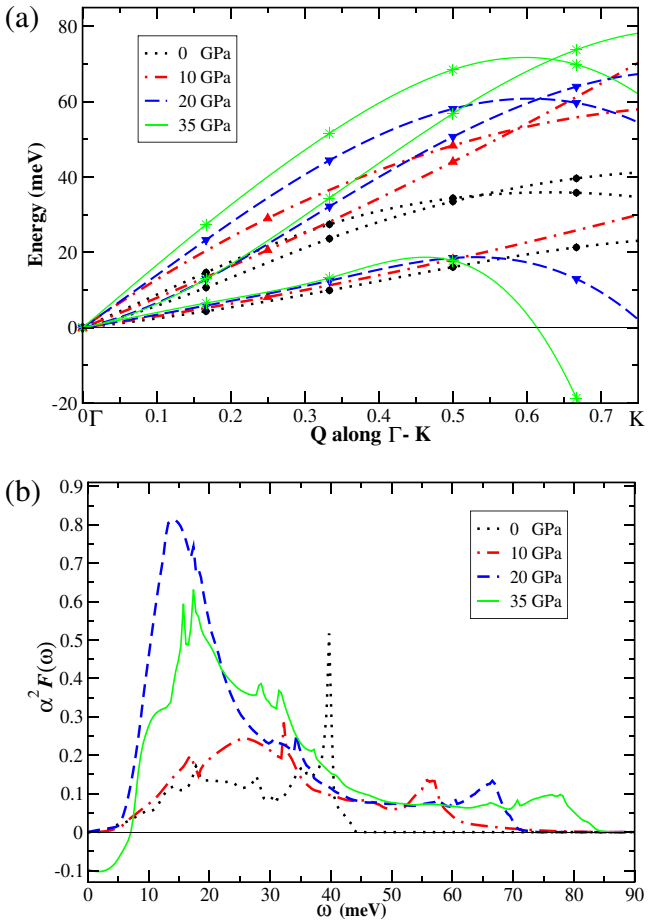

FIG. 3 (color online). (a) Calculated phonon spectrum (interpolated smoothly between calculated points (solid symbols) of fcc Li along the Γ-K direction, at the four pressures indicated. The $\mathcal{T}_1$ (lowest) branch becomes harmonically unstable around K just above 20 GPa. (b) Calculated spectral functions α^2F for $P = 0$, 10, 20, and 35 GPa. Note that, in spite of the (expected) increase in the maximum phonon frequency, the dominant growth in weight occurs in the 10–20 meV region.

Because of the fine structure in $\xi(Q)$ and, hence, in $\lambda_{Q\nu}$, numerically precise results cannot be expected, but general trends should be evident. The resulting spectra are displayed in Fig. 3(b) for each of the four pressures, showing the hardening of the highest frequency $\mathcal{L}$ mode with pressure (43 → 83 meV). The most important change is the growth in weight centered at 25 meV (10 GPa) and then decreasing to 15 meV (20 GPa), beyond which the instability renders any interpretation at 35 GPa questionable. The growing strength is at low energy; note, however, that this region is approaching the energy $\omega_{\text{opt}} = 2\pi k_B T_c \approx$ 10 meV, which Bergmann and Rainer [24] found from calculation of $\delta T_c/\delta\alpha^2F(\omega)$ to be the optimal position to concentrate the spectral weight. These α^2F spectra lead to the values of $\omega_{\log}$, $\langle\omega^2\rangle^{1/2}$, and λ given in Table I. Results from the Allen-Dynes equation [25] (which describes the large λ regime correctly) are shown in Table I

TABLE I. From the calculated $\alpha^2F(\omega)$ at three pressures (P), the logarithmic and second moments of the frequency (K), the value of λ, and T_c (K) calculated using $\mu^* = 0.13$ and $\mu^* = 0.2$.

P (GPa)	$\omega_{\log}$	$\langle\omega^2\rangle^{1/2}$	λ	$T_c(\mu^* = 0.13)$	$T_c(\mu^* = 0.2)$
3	209	277	0.40	0.4	0.01
10	225	301	0.65	5	1.8
20	81	176	3.1	20	16

for the commonly chosen value of Coulomb pseudopotential $\mu^* = 0.13$ as well as for the value $\mu^* = 0.2$ that might be more appropriate for a higher density electron gas. While the low values of T_c are sensitive to μ^*, this sensitivity decreases for large λ and gives values comparable to the observed values.

The calculation of $\xi(Q)$ has shown that Fermi surface topology concentrates scattering processes into well-defined surfaces in Q space and, even in alkali metals, can lead to very strong coupling to specific phonons that can finally drive lattice instability. To enhance λ, it is necessary in addition that the large regions of $\xi(Q)$ are accompanied by large EP matrix elements. We have verified that the $Q = (\frac{2}{3}, \frac{2}{3}, 0)\frac{2\pi}{a}$ $\mathcal{T}_1$ (unstable) phonon (near K) causes large band shifts with atomic displacement ($\delta\varepsilon_k/\delta u \approx 5$ eV/Å) near the FS necks, while for the stable $\mathcal{T}_2$ mode band shifts are no more than 5% of this value. Thus, the focusing of scattering processes is indeed coupled with large, polarization-dependent matrix elements.

This focusing of EP coupling strength makes accurate evaluation of the total coupling strength λ numerically taxing. The richness and strong $\vec{Q}$ dependence of the electron-phonon coupling and the drastic softening at large Q may explain the overestimates of T_c in the previous work on Li that did not take these effects into account, and the same issues may arise in the overestimates in boron [26].

Compressed Li, thus, has several similarities to MgB_2—very strong coupling to specific phonon modes, T_c determined by a small fraction of phonons—but the physics is entirely different, since there are no strong covalent bonds and it is low, not high, frequency modes that dominate the coupling. Compressed Li is yet another system that demonstrates that our understanding of superconductivity arising from "conventional" EP coupling is far from complete, with different systems continuing to unveil unexpectedly rich physics.

We acknowledge important communication with K. Koepernik, A. K. McMahan, and S. Y. Savrasov. This work was supported by National Science Foundation Grants No. DMR-0421810 and No. DMR-0312261. A. L. was supported by the SEGRF program at LLNL, J. K. was supported by DOE Grant No. FG02-04ER46111, and H. R. was supported by DFG (Emmy-Noether-Program).

[1] S. Deemyad and J. S. Schilling, Phys. Rev. Lett. **91**, 167001 (2003).
[2] K. Shimizu *et al.*, Nature (London) **419**, 597 (2002).
[3] V. V. Struzhkin *et al.*, Science **298**, 1213 (2002).
[4] J. Nagamatsu *et al.*, Nature (London) **410**, 63 (2001).
[5] K. I. Juntunen and J. T. Tuoriniemi, Phys. Rev. Lett. **93**, 157201 (2004).
[6] P. B. Allen and M. L. Cohen, Phys. Rev. **187**, 525 (1969).
[7] T. Jarlborg, Phys. Scr. **37**, 795 (1988).
[8] N. E. Christensen and D. L. Novikov, Phys. Rev. Lett. **86**, 1861 (2001).
[9] A. Y. Liu *et al.*, Phys. Rev. B **59**, 4028 (1999).
[10] J. B. Neaton and N. W. Ashcroft, Nature (London) **400**, 141 (1999).
[11] K. Iyakutti and C. Nirmala Louis, Phys. Rev. B **70**, 132504 (2004).
[12] M. Hanfland *et al.*, Nature (London) **408**, 174 (2000); N. E. Christensen and D. L. Novikov, Phys. Rev. Lett. **86**, 1861 (2001).
[13] A. Rodriguez-Prieto and A. Bergara, Proceedings of the Joint 20th AIRAPT-43rd EHPRG 2005 Conference (unpublished).
[14] P. B. Allen, Phys. Rev. B **6**, 2577 (1972); P. B. Allen and M. L. Cohen, Phys. Rev. Lett. **29**, 1593 (1972).
[15] J. An and W. E. Pickett, Phys. Rev. Lett. **86**, 4366 (2001).
[16] J. Kortus *et al.*, Phys. Rev. Lett. **86**, 4656 (2001).
[17] Y. Kong *et al.*, Phys. Rev. B **64**, 020501 (2001).
[18] A. K. McMahan, Phys. Rev. B **29**, 5982 (1984).
[19] We use the local density functional of S. H. Vosko, K. Wilk, and N. Nusair, Can. J. Phys. **58**, 1200 (1980).
[20] L. M. Roth, H. J. Zieger, and T. A. Kaplan, Phys. Rev. **149**, 519 (1966).
[21] T. M. Rice and B. I. Halperin, Phys. Rev. B **1**, 509 (1970).
[22] S. Y. Savrasov, Phys. Rev. B **54**, 16 470 (1996); S. Y. Savrasov and D. Y. Savrasov, *ibid.* **54**, 16 487 (1996).
[23] M. Hanfland *et al.*, Solid State Commun. **112**, 123 (1999).
[24] G. Bergmann and D. Rainer, Z. Phys. **252**, 174 (1972).
[25] P. B. Allen and R. C. Dynes, Phys. Rev. B **12**, 905 (1975).
[26] S. K. Bose *et al.*, Phys. Rev. B **72**, 184509 (2005).